Energy Reports 5 (2019) 1532–1542

Contents lists available at ScienceDirect

Energy Reports

journal homepage: www.elsevier.com/locate/egyr

Research paper

# Solar distillation using three different phase change materials stored in a copper cylinder

Varun Kumar Sonker [a], Jyoti Prasad Chakraborty [b], Arnab Sarkar [a,*], Rishikesh Kumar Singh [a]

[a] Department of Mechanical Engineering, Indian Institute of Technology (B.H.U.), Varanasi, UP 221005, India
[b] Department of Chemical Engineering & Technology, Indian Institute of Technology (B.H.U.), Varanasi, UP 221005, India

ARTICLE INFO

*Article history:*
Received 15 July 2019
Received in revised form 21 October 2019
Accepted 22 October 2019
Available online xxxx

*Keywords:*
Solar distillation
Phase change materials
Solar intensity

ABSTRACT

The present study focuses on the design and fabrication of passive solar still system with phase change materials (PCM). In order to improve the distillate, PCMs (paraffin wax, stearic acid, and lauric acid) have been stored in a copper cylinder. The effects of basin water depth on total distillate have been studied for all three cases. The maximum distillate has been obtained at 1 cm depth for all cases with three PCMs used in this study. Total distillate decreased linearly with water depth for all three PCMs. There has been a 9.2% drop in the maximum water basin temperature in paraffin wax as compared to stearic acid (17.6%) and lauric acid (21.5%) with an increase in water depth from 1 to 5 cm. Heat transfer and energy balance equations involved in the present solar still system have been stated. Variation of some heat transfer coefficients with time has also been studied for three different PCMs. The total distillate has been found to be increased by 1202, 1015, and 930 ml/m$^2$-day for paraffin wax, stearic acid, and lauric acid, respectively stored in a copper cylinder. The performance of lauric acid for total distillate has been comparable with the other two PCMs.



## 1. Introduction

In today's existing scenario of achieving and competing with other developed countries, the developing and underdeveloped nations are facing severe problems to provide adequate and safe drinking water. In 2015 a report was presented by WHO (World health organization) and UNICEF (United Nations International Children's Emergency Fund) that around 663 million people still use unimproved drinking water, which also includes the contaminated wells, springs or unprotected surface water (UNICEF/WHO, 2015). The rapid increase in population and to meet its needs, the usage of fossil fuels has increased to an unprecedented rate leading to environmental issues like greenhouse gas emission and climate change. Also, in recent years, due to significant climate changes, there has been an increase in demand for emergency water supply for drinking purposes in case of crisis or natural calamities such as tsunami, cyclone, and flood (Loo et al., 2012; Xu et al., 2019). During the emergency and crisis conditions, access to electricity becomes very difficult, leading to the need for developing an efficient and portable techniques to obtain a clean source of water. One such technique is solar distillation using phase change material, which operates on a renewable sources of energy.

Now-a-days the provision of pure drinking water is becoming a challenging issue in many areas of the world. In arid and urban areas, drinking water is very scarce, and living of a human being in these areas strongly depends on how much water can be made available. Solar distillation has been in practice for a long time. In the 15th century solar radiation was exposed to water heating, evaporate, and condensate (Nebbia and Menozzi, 1968). In the 16th century, Arab Alchemists carried out the first documented work on solar still (mouchot, 1869). In 1870, the first American patent on solar still was granted for experimental work of Wheeler and Evans (1870). After two years in 1872, Carlos Wilson, an engineer from Sweden, designed and built the first large solar distillation plant in Las Salinas, Chile, for large-scale distilled water production (Talbert et al., 1970). In 1970, Talbert et al. presented the historical background of solar distillation (Talbert et al., 1970), and Delyannis reviewed the major plant of solar still around the world in 1965 (Delyannis, 1965).

In recent years the major development in the field of solar distillation has been found in using thermal energy storage mediums other than water to increase the efficiency of the distillation unit. The thermal energy storage medium helps in stocking the thermal energy in the form of sensible heat or latent heat or both, which can be utilized at a later time for industrial, building,

* Corresponding author.
*E-mail address:* arnab.mec@itbhu.ac.in (A. Sarkar).

https://doi.org/10.1016/j.egyr.2019.10.023

**Nomenclature**

**Symbols**

| | |
|---|---|
| PCM | Phase change material |
| WHO | World health organisation |
| UNICEF | United Nations International Children's, Emergency Fund |
| $A_1$ | Area of water basin ($m^2$) |
| $A_2$ | Area of contact between water and copper cylinder ($m^2$) |
| $A_3$ | Cross section area of cylinder ($m^2$) |
| $A_4$ | Total surface area of cylinder ($m^2$) |
| h | Heat transfer coefficient ($W/m^2$ K) |
| $I_L$ | Solar intensity for lauric acid ($W/m^2$) |
| $I_S$ | Solar intensity for stearic acid ($W/m^2$) |
| $I_P$ | Solar intensity for paraffin wax ($W/m^2$) |
| $T_{aL}$ | Ambient temperature for lauric acid (°C) |
| $T_{aS}$ | Ambient temperature for stearic acid (°C) |
| $T_{aP}$ | Ambient temperature for paraffin wax (°C) |
| $T_{gi}$ | Temperature of glass inner surface (°C) |
| $T_{go}$ | Temperature of glass outer surface (°C) |
| $Q_{Cwg}$ | Convective heat transfer rate from water to glass cover ($W/m^2$) |
| $h_{Cwg}$ | Convective heat transfer coefficient from water to glass cover ($W/m^2$ K) |
| $Q_{ewg}$ | Evaporative heat transfer rate from water to glass cover ($W/m^2$) |
| $h_{ewg}$ | Evaporative heat transfer coefficient from water to glass cover ($W/m^2$ K) |
| $Q_{rwg}$ | Radiative heat transfer rate from water to glass cover ($W/m^2$) |
| $h_{rwg}$ | Radiative heat transfer coefficient from water to glass cover ($W/m^2$ K) |
| $Q_{twg}$ | Total heat transfer rate from water to glass cover ($W/m^2$) |
| $h_{twg}$ | Total heat transfer coefficient from water to glass cover ($W/m^2$ K |
| $Q_{cdgi-go}$ | Conductive heat transfer rate from glass inner surface to outer surface cover |
| $P_{gi}$ | Partial vapour pressure at glass inner surface temperature ($N/m^2$) |
| $T_w$ | Temperature of water (°C) |
| $M_E$ | Equivalent heat capacity (J/K) |
| $P_w$ | Partial vapour pressure of water ($N/m^2$) |
| $K_g$ | Thickness of glass |
| $L_g$ | Thickness of liner |
| k | Thermal conductivity (W/m K) |
| x | Thickness (mm) |
| $\varepsilon_e$ | Effective remittances |

**Greek**

| | |
|---|---|
| $\varepsilon$ | emissivity |
| $\sigma$ | Stefan Boltzmann constant |
| $\alpha$ | Absorptivity |
| $\tau$ | Transmissivity |

**Subs scripts**

| | |
|---|---|
| b | Basin |
| g | Glass |
| r | Radiative |
| $g_i$ | Glass cover inner surface |
| $g_o$ | Glass cover outer surface |
| t | Total |
| w | Water |
| c | copper |
| e | evaporation |
| l | liner |
| m | Mass (kg) |

and solar distillation purposes (Sarbu and Sebarchievici, 2018). The main advantages related to thermal energy storage include an increment in overall efficiency, better economics, lower running cost, and increased reliability. Therefore, the possible use of phase change materials (PCMs) as a thermal energy storage medium in solar system applications are worth investigating. One such application was investigated by Li et al. (2019), where laminated composite PCM blind system was developed, and its performance was measured in a double skin facade (DSF) building. The results revealed that the integrated PCM blind system in DSF kept average air temperature below 35 °C and reduced the inner skin surface temperature of DSF by 2.9 °C, thus reducing heat transfer into the building. Su et al. (2015) reviewed the various types of PCMs in thermal storage applications, and the study revealed that organic PCMs have more advantages in terms of lesser segregation, less super cooling, and broader temperature range application as compared to inorganic PCMs. However, organic PCMs possess some disadvantages, such as lower thermal conductivity, being flammable, and lower density as compared to inorganic PCMs. Su et al. (2017) developed a microencapsulated PCMs, and the results showed better thermal conductivity and higher thermal energy storage density than most of the conventional PCMs when tested for solar assisted hot water storage system. Su et al. (2019a) also investigated the possible use of microencapsulated PCMs for energy storage applications in buildings. The simulation results showed that laminated microencapsulated PCMs drywall performed better as compared to conventional walls over a period of time, with about 12% increase in a number of hours when the indoor air temperature was in the range of 21–28 °C.

Solar stills are broadly divided into passive and active solar stills. Passive solar stills are further divided into a basin and inclined types. Extensive research was reported on different methods to improve the total distillate of these solar stills (Samee et al., 2007; Aybar et al., 2005; Minasian and Al-Karaghouli, 1995; Tiwari et al., 1997; Nafey et al., 2000). The important factors affecting the performance of solar still are solar intensity, the mass of basin water (El-Sebaii, 2004), and wind speed (Tanaka and Nakatake, 2007). We need a safe and reliable energy supply throughout the day. To reduce dependence on non-renewable fossil fuels, such as oil and gas, we also need to make more use of renewable sources like solar and wind. There are two types of solar distillation units one is conventional solar still (without PCM), and the other is solar still integrated with PCM. The basic drawback of conventional solar still is that the system uses only water for its thermal energy storage, making it relatively bulky due to its physical and chemical limitations (Su et al., 2019b). Also, water can absorb solar energy only in the form of sensible

**Table 1**
Thermo-physical properties of PCM Sharma et al. (2009), Farid et al. (2004), Zalba et al. (2003).

| Material properties | Lauric acid | Stearic acid | Paraffin wax |
|---|---|---|---|
| Chemical formula | $(CH_3(CH_2)_{10}COOH)$ | $(CH_3(CH_2)_{16}COOH)$ | $(C_{31}H_{64})$ |
| Melting temperature, °C | 42–46 °C | 52–56 °C | 58–60 °C |
| Latent heat of fusion KJ/kg | 178 | 199 | 226 |
| Solid density, kg/m$^3$ | 862 | 847 | 818 |
| Thermal conductivity, W/m-°C | 0.16 | 0.290 | 0.24 |
| Specific heat capacity, KJ/kg °C | 2.1 | 1.590 | 2.95 |

**Table 2**
Experimental parameters.

| Parameters | Symbols | Value |
|---|---|---|
| Transmittance of cover | $\tau_c$ | 88% |
| Emissivity of cover | $\varepsilon_c$ | 0.97 |
| Wind velocity | V | 1 m/s |
| Density of water | $\rho$ | 989 kg/m$^3$ |
| Latent heat of vaporization | $h_{fg}$ | 2372 (KJ/kg) |
| Declination angle | $\delta$ | 32° |

**Table 3**
Accuracies and range for various instruments.

| S. no. | Instrument | Accuracy | Range |
|---|---|---|---|
| 1 | Solar power meter | 10 W/m$^2$ | 0 – 1999 W/m$^2$ |
| 2 | Digital thermocouple | ±1 °C | −50 – 110 °C |
| 3 | Measuring jar | ±10 ml | 0–2000 ml |
| 4 | Anemometer | 2–4 | 0.4–30 m/s |
| 5 | Hygrometer | ±1 °C | −50 – 70 °C |
| | Ambient temperature | ±10 | 10%–99% |
| | Relative humidity | | |
| 6 | TDS meter | ±2% | 0–5000 ppm (mg/l) |

heat (no phase transformation occurs), and hence, no energy can be obtained once light intensity becomes zero after sunset. However, the solar still integrated with PCM stores solar energy in the form of sensible heat and latent heat due to its phase change phenomenon. As mentioned by Sharma et al. (2009) in their study that PCM can absorb 5–14 times more heat per unit volume as compared to sensible heat storing capacity of water, rock, or masonry. El-Sebaii et al. (2009) also mentioned the appreciable increase in daily productivity from 0.64 (kg/m$^2$-day) to 2.38 (kg/m$^2$-day) for solar still coupled with PCM (stearic acid) as compared to a system without PCM. The main advantages associated with PCM are its low cost, easy availability, suitable phase transforming temperature range, high latent heat of transformation with long term chemical stability, and improved performance in terms of heat transfer and daily productivity.

Phase change materials are also known as latent heat storage materials, which can be used for thermal energy storage, building heating and cooling applications (Kant et al., 2016a; Sharma et al., 2013; Tyagi and Buddhi, 2007), crops drying (Bal et al., 2011, 2010), cooling of photovoltaic (Biwole et al., 2013; Kant et al., 2016b; Huang et al., 2006), electronics cooling and solar greenhouse (Kandasamy et al., 2008; Tan and Tso, 2004; Shukla et al., 2016). According to Kalogirou (1997), in the earliest experimental works, various types of processes that are analysed, the multi-effect boiling system, and multi-effect stack type evaporator are the most suitable for solar energy utilization. Ibrahim et al. (2015) studied a single and double basin type solar still, which is the most widely used for distillation through solar energy. Kumar and Tiwari (1996) found experimentally a single effect active solar still with water flow over the glass cover, which produced the highest distillate. Kabeel (2009) modified the new design for better productivity based on the local climatic condition and operating condition that is a concave wick type evaporation surface. The comprehensive reviews of the solar desalination technique were reported by Tiwari et al. (2003). The simple solar still is the most widely used. However, the main disadvantages of the simple solar sill are low productivity and difficulty to fulfil daily demand for freshwater. Arunkumar et al. (2013) studied the solar still with concentrator-coupled hemisphere basin with and without PCM to enhance the productivity due to heat source of PCM after the sunset and found that PCM became more effective in the low sunshine hours at the low mass of water in the basin. El-Sebaii et al. (2009) achieved the high distillate overnight with a thin layer of stearic acid beneath the basin liner. Moreover, he found PCM to be more effective at a low level of water in the solar still basin. Arunkumar et al. (2013) used spherical copper balls to store PCM in the distillation process. However, for the given volume, the total surface area of a sphere is approximately 14.5% lesser as compared to that of a cylinder. However, in terms of fabrication, achieving a precise dimension for a sphere is difficult as compared to a cylinder made of copper sheet having shallow thickness. The operation of the solar distillation unit mounted with a solar concentrator becomes difficult to operate for the user, as the concentrator has to be adjusted in a regular interval. Tabrizi et al. (2010) and Shukla et al. (2016) used an absorber plate and solar concentrator, respectively, to increase the distillate. Nonetheless, these extra mountings increase the cost of the solar distillation unit, whereas in this study, we have used a simple solar distillation unit with copper cylinders to improve the performance along with making it both user friendly and economically viable.

In the present study, we have analysed the performance of the solar still coupled with three different PCMs having different melting temperature and latent heat capacity. For instance, the thermal performances of PCMs having different melting temperatures like paraffin wax (58–60 °C), stearic (52–56 °C), and lauric acid (42–46 °C) have been compared. In many parts of the world, the intensity of light is less, which can lead to the poor performance of high melting PCMs due to no phase transformation. However, the low melting PCM such as lauric acid (178 kJ/kg) has less latent heat capacity as compared to moderate and high melting PCMs like stearic acid (199 kJ/kg) and paraffin wax (226 kJ/kg), can also adversely affect the solar still performance. Hence, it becomes necessary to compare the performance of different PCMs in solar still in order to predict its feasibility in different regions.

To the best of our knowledge, there is no reported finding regarding the effect of water depth on solar distillation with three different PCMs (lauric acid, stearic acid, and paraffin wax) stored in a copper cylinder. In addition, limited literature has been available for solar distillation, having a copper cylinder for the storage of PCM and stating the physics of its heat transfer with energy balance equations. We have also studied the variation of heat transfer coefficients with time for three different PCMs. Hence, in this study, we have compared the distillate yields at different water depth loaded with three different PCMs stored in six copper cylinders made of 1 mm thick sheet.

**Table 4**
Equation parameters obtained by curve fitting of distillate Vs depth of water.

| PCM | Paraffin wax | Stearic acid | Lauric acid |
|---|---|---|---|
| Residual sum of squares | 5143.9 | 4359.1 | 9294.3 |
| Pearson's r | −0.9931 | −0.99177 | −0.98754 |
| $R^2$ | 0.98625 | 0.9836 | 0.97523 |
| Adj. $R^2$ | 0.98167 | 0.97814 | 0.96698 |
| Linear equation | $\mathbf{Y} = -(192.1 \pm 13.094)\mathbf{X} + (2683.3 \pm 43.423)$ | $\mathbf{Y} = (-161.7 \pm 12.054)\mathbf{X} + (2487.1 \pm 39.978)$ | $\mathbf{Y} = (-191.3 \pm 17.601)\mathbf{X} + (2437.3 \pm 58.377)$ |

*where Y is total distillate and X is depth of water

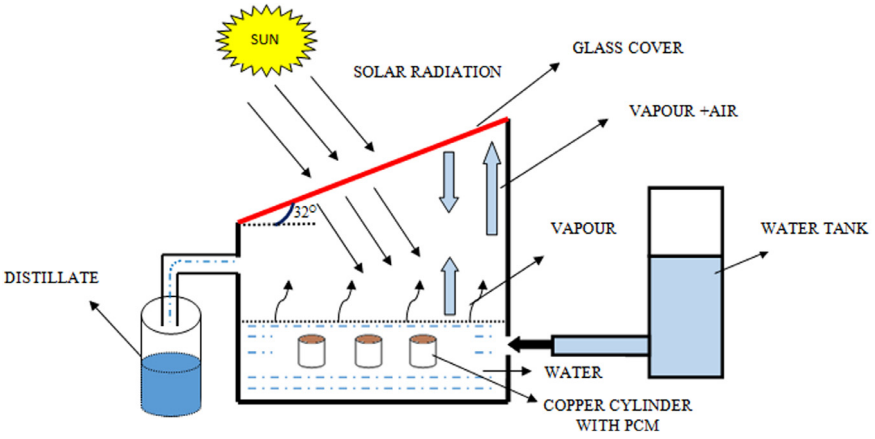


**Fig. 1.** Schematic diagram of passive solar still with PCM.

**Fig. 2.** Pictorial view of the experimental setup for solar still coupled with PCM stored in copper cylinder.

## 2. Materials and methods

### 2.1. Experimental procedure

The schematic and vivid description of the experimental system is shown in Fig. 1. The single slope solar still (75 cm × 75 cm × 15 cm) is made of stainless steel thickness of 1 mm mounted with copper cylinder loaded with PCM. The PCM loaded copper cylinders have been placed in a basin of solar still at a proper distance. Six copper cylinders have been constructed with 7 cm diameter and 7 cm height. Different experiments have been performed in the variation of water depth (1–5 cm) coupled with different PCMs. The experimental parameters involved in the study have been given in Table 2. As depicted in Fig. 1, each copper cylinder has been allowed to fill fully and sealed with high temperature rubber cork. The experiments have been conducted in the month of October from 09.00 am to 08.00 pm. The hourly variations of temperature have been noted by using P-T 100 thermocouples at different points in the solar still. In addition, solar intensity has been measured using solar power metre (accuracy and range of various instruments used in this experiment have been shown in Table 3). The thermo-physical properties of three PCMs used, including their melting and solidifying range is depicted in Table 1 (Sharma et al., 2009; Farid et al., 2004; Zalba et al., 2003). Fig. 2 represents the pictorial view of the experimental set-up used in the present study. Copper cylinders, as depicted in Fig. 3, have been used to store different types of PCMs in order to improve the overall performance due to its higher conductivity, non-corrosive, longer durability, and non-toxic in nature. A commercial grade of lauric acid, stearic acid, and paraffin wax have been used as represented in Fig. 4.

### 2.2. Principles of operation

It can be attributed to Fig. 1 that during charging mode the solar radiation is transmitted through the glass cover, and it is absorbed by the copper cylinder and basin liner resulting in temperature rise. All six copper cylinders in each case have been filled with 1.3 kg of PCM. A part of the energy absorbed by the basin liner as represented in Fig. 1 is transmitted through convection to the basin water. The copper cylinders are heated due to solar radiation and convective heat transfer from water during the charging mode. Heat is first stored as a sensible heat until the PCM reaches its melting point. At this time, PCM starts to melt, resulting in heat storage in the form of latent heat, and after the complete melting of the PCM, the heat will be stored in the melted PCM as sensible heat. After the sunset (discharging mode),

**Fig. 3.** Pictorial view of PCM loaded copper cylinders.


**Fig. 4.** PCM's used in the experiment.

when the solar radiation is zero, the still components start to cool down and the liquid PCM transfers heat to the copper cylinder through conduction mode and from copper cylinder to the basin water through convective mode until the PCM completely solidified and equilibrium temperature is achieved by all components of the solar still. The PCM acts as a heat source for the basin water during the absence of solar intensity. As a consequence, the still continue to produce pure water as collected in the bottle represented in Fig. 1 even after sunset.

### 2.3. Heat transfer and energy balance

Heat transfer in solar still loaded with PCM inside copper cylinder generally depends upon energy transfer between basin liners, basin water, copper cylinder, PCM and glass cover. Solar energy trapped inside the solar still during charging and discharging mode witnesses some losses through glass cover (Singh and Tiwari, 1993; El-Samadony et al., 2016). Heat loss through glass cover occurs mainly in the form of convective, radiative, and evaporative mode. The convective ($h_{cwg}$), radiative ($h_{rwg}$), and evaporative ($h_{ewg}$) heat transfer coefficients can be calculated using Dunkle (1961) correlations. There have been some assumptions made while considering the heat transfer mechanism and energy balance equations. These are as follows:

1. The heat capacities are negligible for basin liner, glass cover, insulating material and copper cylinder as compared to basin water and PCM.
2. Heat transfer from basin liner to the copper cylinder and copper cylinder to glass cover is neglected.
3. The system is considered vapour tight with completely insulated and the side losses are neglected.
4. Heat transfer inside the copper cylinder and PCM is predominantly due to conduction. This is due to the fact that convection does not take place within the copper cylinder when PCM is melted.
5. For simplicity, no thermal gradient is considered throughout the PCM, and its average temperature has been used for all calculations.

#### 2.3.1. Heat loss due to convective heat transfer

The convective mode of heat transfer depends strongly on fluid properties, heat conduction, and slow characteristics. In solar still system coupled with PCM witness convection heat transfer between the water basin surface, and the inner glass cover surface through humid air existing due to temperature difference between them. The convection rate of heat transfer inside the solar still can be calculated using Eq. (1) and is expressed in terms of water temperature ($T_w$) and glass inner

surface temperature ($T_{gi}$).

$$Q_{Cwg} = h_{Cwg} \times (T_w - T_{gi}) \tag{1}$$

where $h_{Cwg}$ is the convective heat transfer coefficient from water to the inner surface of the glass cover, and it can be calculated by Eq. (2) as expressed in Dunkle (1961) correlations.

$$h_{Cwg} = 0.884 \left\{ (T_w - T_{gi}) + \frac{[P_w - P_{gi}]\,[T_w + 273.15]}{[268900 - P_w]} \right\}^{\frac{1}{3}} \tag{2}$$

where $P_w$ and $P_{gi}$ can be calculated using Eqs. (3) and (4) (Dunkle, 1961; Chen et al., 2013):

$$P_w = exp^{\left(25.317 - \frac{5144}{T_w + 273}\right)} \tag{3}$$

$$P_{gi} = exp^{\left(25.317 - \frac{5144}{T_g + 273}\right)} \tag{4}$$

*2.3.2. Heat loss due to radiative heat transfer*

The mechanism involved during the thermal mode of heat transfer includes the emission of internal energy by the object. In the present solar still system, heat transfer due to thermal radiation occurs between the water and inner glass surface separated by medium colder than both bodies. The inclination of glass cover with respect to the water basin is small due to which the view factor between these two surfaces is considered unity. The radiative heat transfer rate ($h_{rwg}$) between glass cover surface and water can be calculated by Eq. (5) (Dunkle, 1961; Chen et al., 2013):

$$Q_{rwg} = h_{rwg} \times \left(T_w - T_{gi}\right) \tag{5}$$

where $h_{rwg}$ is the radiative heat transfer coefficient between the glass cover inner surface and water mass evaluated by Eq. (6):

$$h_{rwg} = \varepsilon_e \sigma \left[ (T_w + 273)^2 + \left(T_{gi} + 273\right)^2 \right] \left(T_w + T_{gi} + 546\right) \tag{6}$$

The effective remittance between glass cover and water mass is expressed as in Eq. (7):

$$\varepsilon_e = \left( \frac{1}{\varepsilon_w} + \frac{1}{\varepsilon_g} - 1 \right) \tag{7}$$

*2.3.3. Heat loss due to evaporative heat transfer*

The vapour pressure is lower as compared to the saturation pressure of the liquid at given temperature evaporation happens between the vapour–liquid interfaces. The evaporative heat transfer occurs between water vapour and water interface (Dunkle, 1961; Chen et al., 2013). The rate of evaporative heat transfer can be expressed as in Eq. (8):

$$Q_{ewg} = h_{ewg} \times (T_w - T_{gi}) \tag{8}$$

where $h_{ewg}$ is evaporation heat transfer coefficient between water mass and inner surface of glass cover, and it can be calculated by Eq. (9):

$$h_{ewg} = 13.273 \times 10^{-3} \times h_{Cwg} \times \left[ \frac{P_w - P_{gi}}{T_w - T_{gi}} \right] \tag{9}$$

The total heat transfer rate ($Q_{twg}$) can be expressed as in Eqs. (10) and (11):

$$Q_{twg} = Q_{Cwg} + Q_{rwg} + Q_{ewg} \tag{10}$$

$$Q_{twg} = h_{twg} \times (T_w - T_{gi}) \tag{11}$$

The total internal heat transfer coefficient between the water mass and the inner surface of the glass cover ($h_{twg}$) can be calculated as given in Eq. (12):

$$h_{twg} = h_{Cwg} + h_{rwg} + h_{ewg} \tag{12}$$

The conductive heat transfer rate through the glass cover thickness from its inner surface to the outer surface can be expressed as in Eq. (13):

$$Q_{cdgi-go} = \frac{K_g}{L_g} \left(T_{gi} - T_{go}\right) \tag{13}$$

*2.3.4. Solar still with the PCM (charging mode)*

In the present solar still system during the charging mode, heat transfer occurs between the water basin, and copper cylinder and the energy balance equation during the sunshine hours may be expressed as in Eq. (14):

For water basin

$$h_{lw}A_1\,(T_l - T_w) + I\tau_g\alpha_w A_1 = A_1 h_t \left(T_w - T_g\right) + h_{wc}A_2\,(T_w - T_c) + m_w C_w \frac{dT_w}{dt} \tag{14}$$

where $A_1$ is the area of the water basin, and $A_2$ is an area of contact between water and copper cylinder.

On the basis of stated assumptions in Section 2.3. The energy balance between basin liner and water can be expressed as in Eq. (15):

$$I\tau_g\tau_w\alpha_l = h_{lw}(T_l - T_w) \tag{15}$$

During the charging mode, heat transfer occurs between PCM and water basin via copper cylinder. The energy balance equation for the copper cylinder is given by Eq. (16):

$$I\tau_g\alpha_c A_3 + h_{wc}A_2\,(T_w - T_c) = A_4 \frac{K_c}{X_c} \left(T_c - T_{pcm}\right) \tag{16}$$

where $A_3$ is cross-sectional area, and $A_4$ is the total surface area of the copper cylinder.

PCM during the charging mode stores solar energy in the form of sensible heat and latent heat of fusion. On the basis of assumptions made, the heat transfer between PCM and copper cylinder occurs mainly due to conduction, and energy balance for PCM can be expressed as in Eq. (17):

$$A_4 \frac{K_c}{X_c} \left(T_c - T_{pcm}\right) = M_E \frac{dT_{pcm}}{dt} \tag{17}$$

where $M_E$ is the equivalent heat capacity, and it can be given as:

$M_E = m_{pcm}C_s$ for $T_{pcm} < T_m$

$M_E = m_{pcm}L_s$ for $T_{pcm} = T_m$

$M_E = m_{pcm}C_l$ for $T_{pcm} > T_m$

*2.3.5. Solar still with the PCM (discharging mode)*

In the absence of solar radiation as the temperature of the water, basin decreases, solidification (phase change) of PCM happens to result in net heat transfer from PCM to water basin via copper cylinder. As the temperature difference between liner and water basin is negligible during discharging mode; hence, heat transfer between them can be neglected.

Based on assumptions made, the energy balance equations for water basin during Sunset hours can be expressed as in Eq. (18):

$$h_{wc}A_2\,(T_c - T_w) = A_1 h_t \left(T_w - T_g\right) + m_w C_w \frac{dT_w}{dt} \tag{18}$$

The energy balance equation for copper cylinder during discharging mode can be given by Eq. (19):

$$A_4 \frac{K_c}{X_c} \left(T_{pcm} - T_c\right) = h_{wc}A_2\,(T_c - T_w) \tag{19}$$

During sunset hours heat transfer occurs from PCM to copper cylinder, and as a convective mode of heat transfer between them

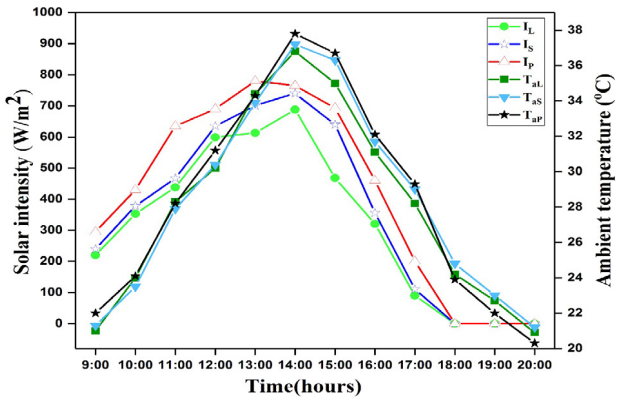


**Fig. 5.** Intensity and ambient temperature variation for different PCM's.

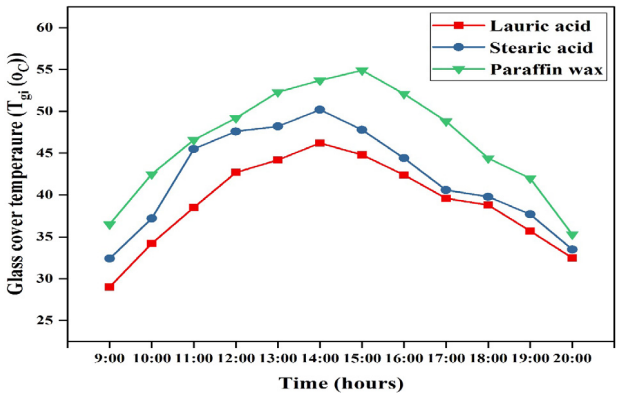


**Fig. 6.** Variations of glass cover temperature for three different PCM's.

can be neglected, the energy balance equation for PCM is given by Eq. (20):

$$M_E \frac{dT_{pcm}}{dt} = A_4 \frac{K_{pcm}}{X_{pcm}} \left(T_{pcm} - T_c\right) \tag{20}$$

where $M_E$ is the equivalent heat capacity and can be expressed as:

$$M_E = m_{pcm} C_s \quad \text{for } T_{pcm} < T_m$$
$$M_E = m_{pcm} L_s \quad \text{for } T_{pcm} = T_m$$
$$M_E = m_{pcm} C_l \quad \text{for } T_{pcm} > T$$

## 3. Results and discussion

### 3.1. Variation of solar intensity, ambient temperature and glass cover temperature with time

The solar still performance with the phase change materials has been studied in the month of October when the intensity of solar radiation is low as compared to summer. Fig. 5 depicts the variation of solar radiation and ambient temperature with respect to the time, and average values have been quoted for the course of five different depth of water for respective PCMs. In this study $I_L$, $I_S$, and $I_P$ represents solar intensity for lauric acid, stearic acid and paraffin wax, respectively. $T_{aL}$, $T_{aS}$, and $T_{aP}$ show the ambient temperature for lauric acid, stearic acid, and paraffin wax, respectively. Fig. 6 represents the glass cover temperatures ($T_g$) for three different PCMs, and average values have been stated in this study for the course of five different depths. It can be illustrated that glass temperature increases with time and reaches a maximum temperature between 01:00–2:00 PM. It has been obvious that in the early hours of the day the inner glass temperature is close to that of water basin temperature. However, as the day, progresses the difference increases due to the fact that water can absorb some of the incident solar energy, whereas glass transmits most of the incident solar intensity.

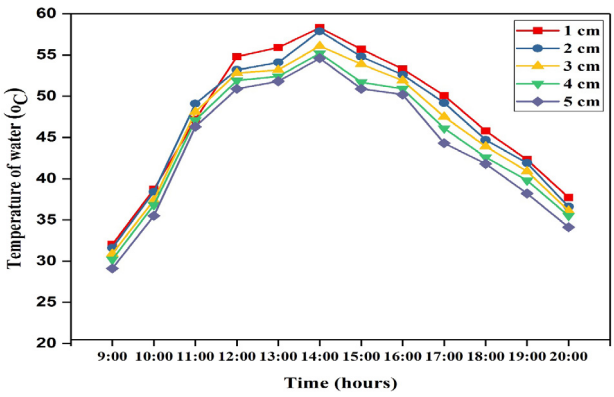


**Fig. 7.** Temperature of water basin coupled with lauric acid.

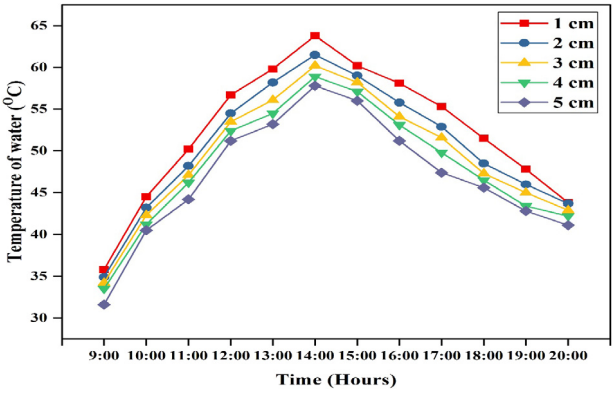


**Fig. 8.** Temperature of water basin coupled with stearic acid.

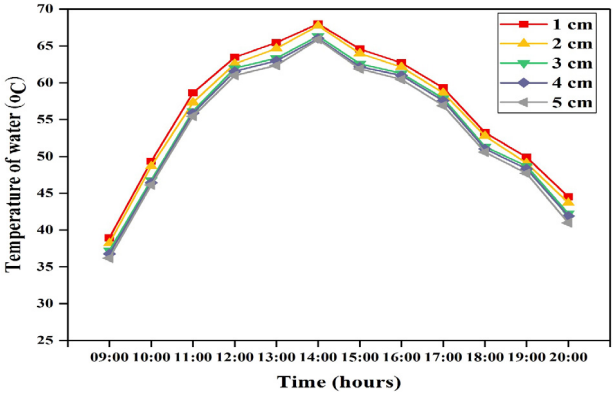


**Fig. 9.** Temperature variation of water basin coupled with paraffin wax.

### 3.2. Variation of water basin temperature with depth of the water

In Figs. 7, 8 and, 9 it can be noted that the maximum temperature attained by the water basin decreases with an increase in depth of water. It can also be observed that for paraffin wax there has been 9.2% drop in the maximum water basin temperature as compared to stearic acid (17.6%) and lauric acid (21.5%) when the water depth has been increased from 1 cm to 5 cm. The decrease

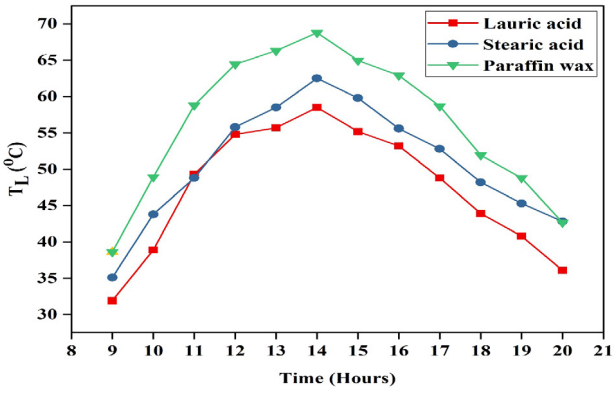


**Fig. 10.** Temperature variation of liner for three different PCM's.

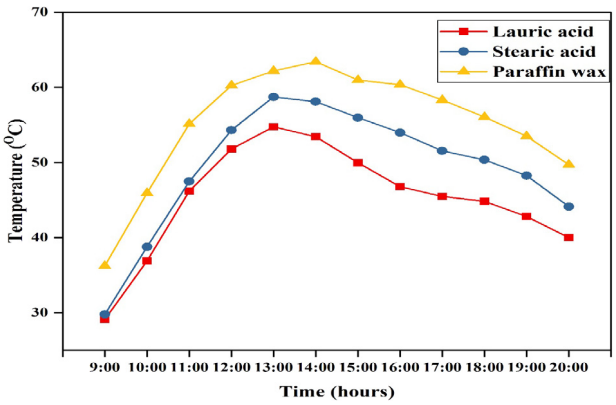


**Fig. 11.** Hourly temperature variation of PCM's.

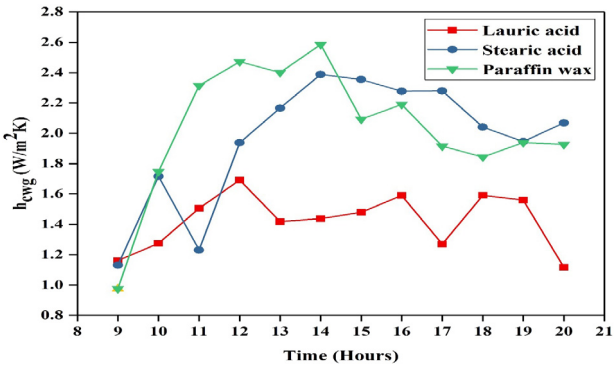


**Fig. 12.** Convective heat transfer coefficient from water to glass cover with respect to time.

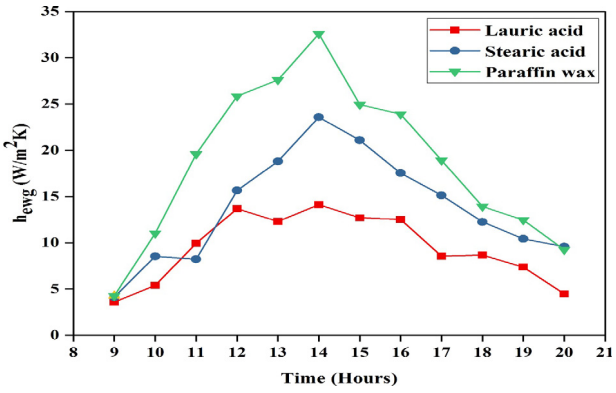


**Fig. 13.** Evaporative heat transfer coefficient from water to glass cover with respect to time.

in water basin temperature with an increase in depth of water has been due to the fact that the amount of water in the basin increased. After sunset due to lack of radiation, the temperature of water in the basin decreases slowly due to the use of stored heat energy from the PCM. The variation between water basin temperatures in all three cases at different water depths has also been due to some environmental conditions like fluctuation in solar radiation, wind speed, ambient temperature, and spatial wind barriers.

As the day progresses in the first half, water temperature increases faster as compare to the glass temperature due to expose of glass surface to the ambient atmosphere. Alteration in glass and water temperature can be attributed to unstable climatic conditions. However, in all cases, the pattern followed by the curves in Figs. 6, 7, 8, and 9 have a similarity.

### 3.3. Temperature variation of PCM and basin liner

The hourly variation of liner temperature for different PCMs has been represented in Fig. 10. The average maximum temperature over the course of five different depths has been 68.8, 62.5, and 58.5 °C for paraffin wax, stearic, and lauric acid, respectively. Basin liner has been painted black for the fact that it can absorb maximum incident solar radiation after some of the radiation is lost through glass cover while some have been absorbed by the water basin.

Fig. 11 indicates PCM temperature for three different PCMs. It can be observed that $T_{PCM}$ increases with time as the solar radiation increases. Sensible heat is stored in the form of thermal energy in the solid PCM until it reaches the melting point. The melting point of paraffin wax is about 59 °C, whereas for lauric and stearic acid, it is about 44 °C and 54 °C, respectively. Then $T_{PCM}$ continues to be constant for some time interval during the noontime as the PCM undergoes phase transformation. Once complete phase transformation occurs, the $T_{PCM}$ again increases due to sensible heat storage in liquid form. Maximum temperature achieve by PCMs have been 53.4 °C (lauric acid), 58.1 °C (stearic acid) and 63.4 °C (paraffin wax). As the temperature increased beyond the melting point in all three cases confirmed that the complete melting of PCMs occurred during the experiment. However, Tabrizi et al. (2010) observed in their study that the complete melting of PCM did not occur and this suggests that in our study, the PCMs have been stored in copper cylinders resulted in better heat transfer. It can also be observed that once the discharging process started at constant temperature unless PCM completely solidified and afterwards $T_{PCM}$ decreases gradually with time in all three cases. It is seen that the $T_{PCM}$ increases with time due to the increased rate of heat transfer by conduction from the basin liner to the PCM as the solar radiation intensity increases. The PCM starts melting after achieving its melting point temperature from exposure to solar radiation at a higher level. Afterwards, $T_{PCM}$ decreases slowly with time after sunset when the discharging process of heat stored within the PCM begins.

### 3.4. Variation of heat transfer coefficient for different PCMs

It can be observed from Figs. 12–16, that heat transfer coefficient ($h_{cwg}$, $h_{ewg}$, $h_{rwg}$, $h_t$, and $h_{lw}$) varies with time for all solar still components. In this study, we have calculated the heat transfer coefficient for water to glass during the observed period as most of the losses in the solar still occurs through

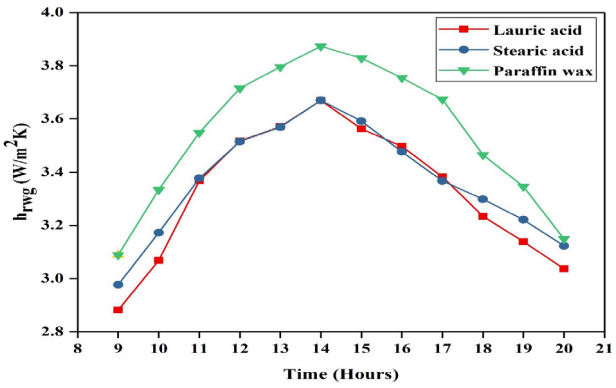


**Fig. 14.** Radiative heat transfer coefficient from water to glass cover with respect to time.

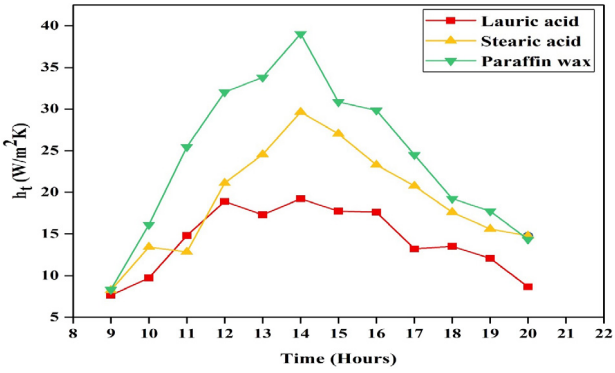


**Fig. 15.** Total heat transfer coefficient from water to glass cover with respect to time.

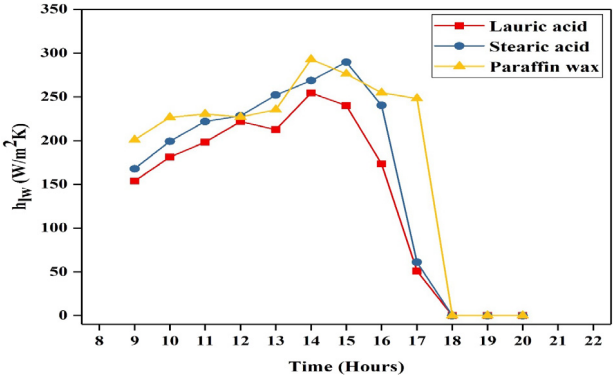


**Fig. 16.** Heat transfer coefficient from liner to water with respect to time.

glass cover (as no heat loss is considered from insulation side). In Figs. 12–15, the heat transfer coefficient is more for paraffin wax followed by stearic acid and lauric acid due to the fact that incident solar radiation in case of paraffin wax has been higher and the temperature difference between glass cover temperature, and water is less during the charging mode. There was no proper trend followed in the case of the heat transfer coefficient from liner to water due to the fact that there has been no influence of PCM property on heat transfer mechanism occurring between liners to water. After sunset, as the temperature of liner and water becomes approximately equal, the heat transfer coefficient ($h_{lw}$) becomes zero.

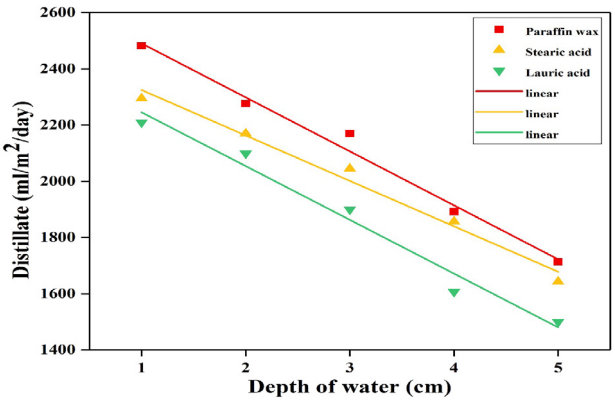


**Fig. 17.** Variation of total distillate with depth of water.

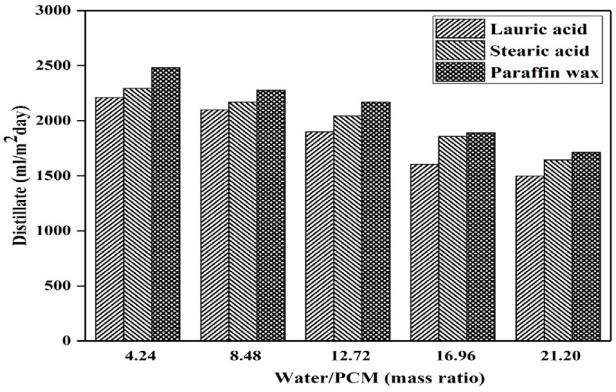


**Fig. 18.** Variation of (daily yield) vs (water mass/PCM mass).

### 3.5. Variation of total distillate with water depth and validation

Fig. 17 indicates the daily total distillate at the different levels of water depth (1–5 cm) and Fig. 18 represents the total daily distillate versus mass ratio (Water/PCM). The maximum daily distillate obtained for paraffin wax, stearic acid, and lauric acid have been 2482. 2295, and 2210 ml/m$^2$-day, respectively. It can also be observed that maximum output has been obtained at 1 cm for all three PCMs. This was because as the water depth increases the amount of water in the basin increases leading to lower water temperature as shown in Figs. 7, 8, and 9. A clear trend can be asserted that with an increase in depth, total distillate decreases. Table 4 represents the parameters and linear equation obtained after the curve fitting of the experimental data. The curve fitting having $R^2$ and adjusted $R^2$ value greater than 0.95 is acceptable, suggesting that the obtained linear equation can explain 95% of the data variability (Buratti et al., 2018; Bajar et al., 2016). Pearson's r represents the relationship between X (water depth) and Y (distillate) variables. Its value lies between −1 to +1. As can be observed from Table 4 that all three curves, Pearson's r-value lie closed to −1, suggesting that Y decreases when X increases.

Fig. 19 represents the comparison of the increase in distillate due to PCM with the other two studies carried out by Arunkumar et al. (2013) and Tabrizi et al. (2010). In our study, total distillate without PCM has been 1298 ml/m$^2$-day at 1 cm depth Whereas, the increase in distillate due to PCM at 1 cm depth have been 1202 (paraffin wax), 1015 (stearic acid) and 930 (lauric acid) ml/m$^2$-day as compared to 940 (Arunkumar et al., 2013) and 290 ml/m$^2$-day (Tabrizi et al., 2010). It is quite clear that in our study the increase in distillate for paraffin wax and stearic acid has been found to be greater than the other two studies. However,

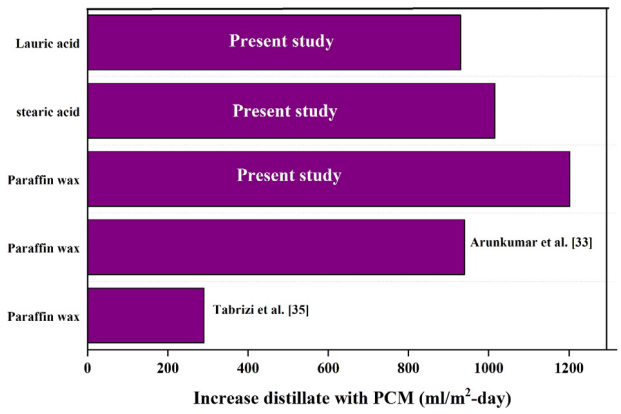


**Fig. 19.** Comparison of increased distillate with PCM.

for lauric acid, the increase in the distillate is also adequate, giving major scope for regions with lower radiation and ambient temperature. This is due to the fact that lauric acid (42–46 °C) has a much lower melting point as compared to paraffin wax (58–60 °C) and stearic acid (52–56 °C).

## 4. Conclusions

Producing fresh water by solar still with its simplicity would be one of the best solutions to supply freshwater with limited technical facilities in remote areas, especially in crises. Copper cylinders filled with phase change materials integrated above the basin liner improved the productivity of the solar still. Water basin temperature decrease with an increase in water depth using paraffin wax, which is being least affected due to high heat storing capacity as compared to stearic and lauric acid. Total distillate decreased linearly with the water depth in all three PCMs. The maximum distillate has been obtained using paraffin wax as compared to stearic acid and lauric acid. This has been due to the high latent heat of capacity of paraffin wax as compared to the other two PCMs. However, lauric acid still also performed well as the other two PCMs when stored in a copper cylinder. Cylindrical storage for PCM has rendered better results as compared to spherical storage due to its high surface area.

## Declaration of competing interest

The authors declare that they have no known competing financial interests or personal relationships that could have appeared to influence the work reported in this paper.

## Acknowledgment

The authors acknowledge the funding from SERB, New Delhi, India through fund no. SR/FTP/ETA-56/2012.

## References

Arunkumar, T., et al., 2013. The augmentation of distillate yield by using concentrator coupled solar still with phase change material. Desalination 314, 189–192.
Aybar, H.Ş, Egelioğlu, F., Atikol, U., 2005. An experimental study on an inclined solar water distillation system. Desalination 180 (1), 285–289.
Bajar, S., et al., 2016. Evaluation and statistical optimization of methane oxidation using rice husk amended dumpsite soil as biocover. Waste Manag. 53, 136–143.
Bal, L.M., Satya, S., Naik, S.N., 2010. Solar dryer with thermal energy storage systems for drying agricultural food products: A review. Renew. Sustain. Energy Rev. 14 (8), 2298–2314.
Bal, L.M., et al., 2011. Review of solar dryers with latent heat storage systems for agricultural products. Renew. Sustain. Energy Rev. 15 (1), 876–880.
Biwole, P.H., Eclache, P., Kuznik, F., 2013. Phase-change materials to improve solar panel's performance. Energy Build. 62, 59–67.
Buratti, C., et al., 2018. Optimization of torrefaction conditions of coffee industry residues using desirability function approach. Waste Manag. 73, 523–534.
Chen, Z., et al., 2013. Analysis of the characteristics of heat and mass transfer of a three-effect tubular solar still and experimental research. Desalination 330, 42–48.
Delyannis, A.A., 1965. Solar stills provide an island's inhabitants with water. Sun Work 10 (1).
Dunkle, R.V., 1961. International development in heat transfer. In: ASME Proceedings. Inter. Heat Transfer. University of Colorado, p. 895, Part V.
El-Samadony, Y.A.F., El-Maghlany, W.M., Kabeel, A.E., 2016. Influence of glass cover inclination angle on radiation heat transfer rate within stepped solar still. Desalination 384, 68–77.
El-Sebaii, A.A., 2004. Effect of wind speed on active and passive solar stills. Energy Convers. Manage. 45 (7), 1187–1204.
El-Sebaii, A.A., et al., 2009. Thermal performance of a single basin solar still with PCM as a storage medium. Appl. Energy 86 (7), 1187–1195.
Farid, M.M., et al., 2004. A review on phase change energy storage: materials and applications. Energy Convers. Manage. 45 (9), 1597–1615.
Huang, M.J., Eames, P.C., Norton, B., 2006. Phase change materials for limiting temperature rise in building integrated photovoltaics. Sol. Energy 80 (9), 1121–1130.
Ibrahim, A.G.M., Allam, E.E., Elshamarka, S.E., 2015. A modified basin type solar still: Experimental performance and economic study. Energy 93, 335–342.
Kabeel, A.E., 2009. Performance of solar still with a concave wick evaporation surface. Energy 34 (10), 1504–1509.
Kalogirou, S., 1997. Survey of solar desalination systems and system selection. Energy 22 (1), 69–81.
Kandasamy, R., Wang, X.-Q., Mujumdar, A.S., 2008. Transient cooling of electronics using phase change material (PCM)-based heat sinks. Appl. Therm. Eng. 28 (8), 1047–1057.
Kant, K., Shukla, A., Sharma, A., 2016a. Performance evaluation of fatty acids as phase change material for thermal energy storage. J. Energy Storage 6, 153–162.
Kant, K., et al., 2016b. Heat transfer studies of photovoltaic panel coupled with phase change material. Sol. Energy 140, 151–161.
Kumar, S., Tiwari, G.N., 1996. Performance evaluation of an active solar distillation system. Energy 21 (9), 805–808.
Li, Y., et al., 2019. Phase change material blind system for double skin façade integration: System development and thermal performance evaluation. Appl. Energy 252, 113376.
Loo, S.-L., et al., 2012. Emergency water supply: A review of potential technologies and selection criteria. Water Res. 46 (10), 3125–3151.
Minasian, A.N., Al-Karaghouli, A.A., 1995. An improved solar still: The wick-basin type. Energy Convers. Manage. 36 (3), 213–217.
mouchot, Augustin, 1869. l.c.s., Applications industrielles Solar Energy The French Connection part one.
Nafey, A.S., et al., 2000. Parameters affecting solar still productivity. Energy Convers. Manage. 41 (16), 1797–1809.
Nebbia, G., Menozzi, G.N., 1968. Early experiments on water desalination by freezing. Desalination 5 (1), 49–54.
Samee, M., et al., 2007. Design and Performance of a Simple Single Basin Solar Still, Vol. 11. pp. 543–549.
Sarbu, I., Sebarchievici, C., 2018. A comprehensive review of thermal energy storage. Sustainability 10 (1), 191.
Sharma, A., et al., 2009. Review on thermal energy storage with phase change materials and applications. Renew. Sustain. Energy Rev. 13 (2), 318–345.
Sharma, A., et al., 2013. Development of phase change materials for building applications. Energy Build. 64, 403–407.
Shukla, A., Sharma, A., Kant, K., 2016. Solar greenhouse with thermal energy storage: a review. Curr. Sustain. Renew. Energy Rep. 3 (3–4), 58–66.
Singh, A.K., Tiwari, G.N., 1993. Thermal evaluation of regenerative active solar distillation under thermosyphon mode. Energy Convers. Manage. 34 (8), 697–706.
Su, W., Darkwa, J., Kokogiannakis, G., 2015. Review of solid–liquid phase change materials and their encapsulation technologies. Renew. Sustain. Energy Rev. 48, 373–391.
Su, W., Darkwa, J., Kokogiannakis, G., 2017. Development of microencapsulated phase change material for solar thermal energy storage. Appl. Therm. Eng. 112, 1205–1212.
Su, W., Darkwa, J., Kokogiannakis, G., 2019a. Numerical thermal evaluation of laminated binary microencapsulated phase change material drywall systems. Build. Simul..
Su, W., et al., 2019b. Microencapsulation of paraffin with poly (Urea Methacrylate) shell for solar water heater. Energies 12 (18), 3406.
Tabrizi, F.F., Dashtban, M., Moghaddam, H., 2010. Experimental investigation of a weir-type cascade solar still with built-in latent heat thermal energy storage system. Desalination 260 (1), 248–253.

Talbert, S.G., et al., 1970. Manual on Solar Distillation of Saline Water. U.S. Office of Saline Water. Research and Development Progress Report, no. 546, U.S. Dept. of the Interior : Distributed by National Technical Information Service. x, Washington, D.C., p. 263.
Tan, F.L., Tso, C.P., 2004. Cooling of mobile electronic devices using phase change materials. Appl. Therm. Eng. 24 (2), 159–169.
Tanaka, H., Nakatake, Y., 2007. Effect of inclination of external flat plate reflector of basin type still in winter. Sol. Energy 81 (8), 1035–1042.
Tiwari, G.N., Kupfermann, A., Aggarwal, S., 1997. A new design for a double-condensing chamber solar still. Desalination 114 (2), 153–164.
Tiwari, G.N., Singh, H.N., Tripathi, R., 2003. Present status of solar distillation. Sol. Energy 75 (5), 367–373.
Tyagi, V.V., Buddhi, D., 2007. PCM thermal storage in buildings: A state of art. Renew. Sustain. Energy Rev. 11 (6), 1146–1166.
UNICEF/WHO, 2015. Progress on Sanitation and Drinking Water – 2015 Update and MDG Assessment. WHO Library Cataloguing-in-Publication Data.
Wheeler, N.W., Evans, W.W., 1870. Evaporating and distilling with solar heat. US Patent No. 102633.
Xu, Y., et al., 2019. Origami system for efficient solar driven distillation in emergency water supply. Chem. Eng. J. 356, 869–876, Water Res. 46 2012.
Zalba, B., et al., 2003. Review on thermal energy storage with phase change: materials, heat transfer analysis and applications. Appl. Therm. Eng. 23 (3), 251–283.